Dynamic scaling form in wavelet-discriminated Edwards-Wilkinson growth equation

Z. Moktadir*
School of Electronics and Computer Science, Southampton University, United Kingdom
(Received 16 March 2005; published 28 July 2005)

We present an analysis of dynamic scaling of the Edwards-Wilkinson growth model from wavelets' perspective. Scaling function for the surface width is determined using wavelets' formalism, by computing the surface width for each wavelet scale, we show that an exact and simple form of the scaling function is obtained. These predictions are confirmed by computer simulation of a growth model described by the EW equation, and by numerical calculations.

DOI: 10.1103/PhysRevE.72.011608 PACS number(s): 81.15.Aa, 05.40.−a, 68.35.Ct, 68.55.Jk

I. INTRODUCTION

Growth of smooth thin films has major implications in the microelectronics industry and nanotechnology. Understanding the mechanisms by which surfaces and interfaces roughen during growth, was the subject of an enormous theoretical and experimental effort in recent years [1–4]. Nonequilibrium growth models were developed either as computer simulations or as continuum stochastic, partial differential equations. In continuum models, surface roughening is caused by fluctuations in the flux of deposited atoms, and fluctuations of the surface obey dynamic scaling laws. A quantity which is often investigated, and obeying such laws, is the surface width ω which is expected to be in the form

$$\omega(L,t) = L^{\alpha} f(t/L^{z}), \tag{1}$$

where L is the length over which ω is calculated (or measured), t is the time, α is the roughness exponent, and $z=\alpha/\beta$ is the dynamic exponent. The scaling function f has the asymptotic form, $f \sim x^{\beta}$ for $x \ll 1$ and $f=$const for $x \gg 1$. The simplest equation that describes a variety of surface dynamics is the Edwards-Wilkinson equation [5] which is given by

$$\frac{\partial h}{\partial t} = \nu \nabla^2 h + \eta(\mathbf{x},t), \tag{2}$$

where ν is often called the surface tension and $\eta(\mathbf{x},t)$ is the random component of the incoming flux, which is a function of the position and time. This function is assumed to be a Gaussian white noise with zero mean, or a spatially correlated noise (long-ranged correlation), i.e.,

$$\langle \eta(\mathbf{x},t)\, \eta(\mathbf{x}',t') \rangle = 2F \delta(\mathbf{x}-\mathbf{x}')\, \delta(t-t'), \tag{3}$$

$$\langle \eta(\mathbf{x},t)\, \eta(\mathbf{x}',t') \rangle = 2F |\mathbf{x}-\mathbf{x}'|^{2\rho-d} \delta(t-t'), \tag{4}$$

where F is a constant and $0<\rho<1/2$ is an exponent characterizing the decay of spatial correlations. The respective Fourier transforms are given by

$$\langle \eta(\mathbf{q},t)\, \eta(\mathbf{q}',t') \rangle = 2F \delta(\mathbf{q}+\mathbf{q}')\, \delta(t-t'), \tag{5}$$

$$\langle \eta(\mathbf{q},t)\, \eta(\mathbf{q}',t') \rangle = 2D_{\rho} q^{-2\rho} \delta(\mathbf{q}+\mathbf{q}')\, \delta(t-t'). \tag{6}$$

At $d=1$, the prefactor D_{ρ} is given by

$$D_{\rho} = \frac{F}{\pi} \int_0^{\infty} u^{2\rho-1} \cos(u) du = \frac{F 2^{2\rho-1} \sqrt{\pi}\, \Gamma(\rho)}{\Gamma(1/2-\rho)}, \tag{7}$$

where Γ is the gamma function. Equation (2) is soluble and the corresponding dynamic and roughness exponent in one-dimensional space for uncorrelated noise are $z=2$ and $\alpha=1/2$, respectively. For a spatially correlated noise, the exponents are $\alpha=\rho+1/2$ and $z=2$ in one-dimensional space. These exponents are obtained either by using scaling arguments or solving the growth equation exactly. Usually this is achieved using Fourier methods [6–10], leading to complicated scaling functions for which asymptotic form is given. We propose in this paper to investigate the EW equation using wavelets formalism. We will show that simple form of the scaling function is obtained in two cases, growth with noncorrelated noise; and growth with spatially correlated noise.

Wavelets can decompose a surface profile concisely given information on both, the scale and the location simultaneously. We will investigate the scaling of the surface width at each scale instead of investigating it as a function of the system size, as it is usually performed. Finally, we will compare our analytical results to a computer model described by the EW equation and to numerical calculations.

II. WAVELET DECOMPOSITION OF EW EQUATION

Wavelet analysis is the breaking up of a signal into shifted and scaled versions of the original (or mother) wavelet. That is,

$$\psi(a,b) = \frac{1}{\sqrt{a}} \psi\left(\frac{x-b}{a}\right) \tag{8}$$

where a ($a>0$) and b are, respectively, the scale parameter and the dilatation parameter, x is the space variable, and ψ is the mother wavelet. These basis functions vary in scale by slicing the data space using different scale sizes. The continuous wavelet transform (CWT) is defined as the sum over all of the surface profile multiplied by the shifted and scaled mother wavelet,

*Electronic address: zm@ecs.soton.ac.uk

 ©2005 The American Physical Society

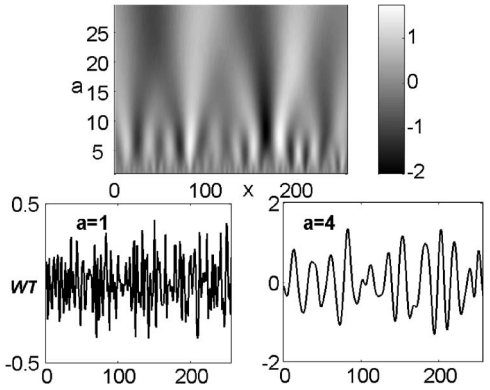

FIG. 1. Wavelet transform of the surface profile obtained by numerically solving the EW equation. The top graphic shows two-dimensional gray scale representation of $W_T(a,x)$. The bottom graphs show slices of $W_T(a,x)$ for two different scales $a=1$, and $a=4$.

$$W_T(a,b) = \int h(x)\psi(a,b)dx, \tag{9}$$

$W(a,b)$ are the wavelet coefficients which are a function of the scale and the position. Then, CWT describes the surface profile in a given position b and a given scale a.

Since the height $h(x)$ is assumed to be a single valued function of x, it is possible to perform its wavelet transform, i.e.,

$$W_T(a,x) = \frac{1}{\sqrt{a}} \int h(y)\psi\left(\frac{y-x}{a}\right)dy. \tag{10}$$

Thus, wavelets have the ability to split a surface profile up into components that are not pure sine waves, as opposed to Fourier transform. When summing all those components, one retrieves the exact profile. In Fig. 1 we show two-dimensional grey scale representation of the wavelet transform of the surface profile generated by Eq. (2) and the decomposition of the surface profile at the scales $a=1$ and $a=4$. These profiles are obtained by applying Eq. (10) to Eq. (2). Notice that small scales correspond to the details (high frequencies) of the surface profile and large scales correspond to the large features (low frequencies) of the surface profile. It should also be noted that the decomposition does not result in sine waves like in Fourier expansion. In this calculation we used the well-known *Mexican hat* wavelet which is given by $\psi(x)=(1-x^2)\exp(-x^2/2)$. The wavelet $\psi(x)$ and its Fourier transform are displayed in Fig. 2.

III. DYNAMIC SCALING

In this section the lateral system size L is taken to be infinite and therefore the dependence on L is suppressed. We also restrict ourselves to one-dimensional space. Since each decomposition does not result in a sine wave, it is possible to calculate its power spectrum. By setting $\xi=(y-x)/a$ in Eq. (10), we compute the Fourier transform of each decomposition,

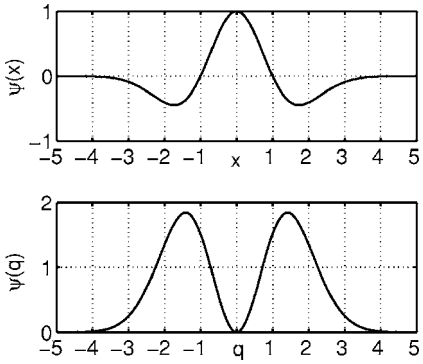

FIG. 2. Top graphic, Gaussian wavelet of order 2 and its Fourier transform, bottom graphic.

$$\hat{W}(a,q,t) = -\sqrt{a}\hat{h}(q,t)\int \psi(\xi)e^{iq\xi}d\xi = -\sqrt{a}\hat{h}(q,t)\hat{\psi}(-aq), \tag{11}$$

where $\hat{h}$ and $\hat{\psi}$ are the Fourier transforms of the height h and the mother wavelet ψ, respectively. The power spectrum of each decomposition is then

$$\Gamma(a,q,t) = \langle \hat{W}(a,q,t)\hat{W}(a,-q,t)\rangle = aP(q,t)|\hat{\psi}(-aq)|^2. \tag{12}$$

The function $\hat{\psi}(q)$ is the Fourier transform of the mother wavelet. For the "Mexican hat" wavelet $\psi(x)$, the function $\hat{\psi}(q)$ is given by $\hat{\psi}(q)=\sqrt{2\pi}q^2\exp(-q^2/2)$ which is displayed in Fig. 2. The quantity $P(q)$ is the power spectrum of the surface height. By applying Fourier-transforming equation (2), we obtain

$$\frac{\partial \hat{h}}{\partial t}(q,t) = -\nu q^2\hat{h}(q,t) + \hat{\eta}(q,t), \tag{13}$$

where $\hat{h}(q,t)$ and $\hat{\eta}(q,t)$ are the Fourier transforms of the height h, and the noise η, respectively. Equation (13) is trivial and its solution is given by

$$\hat{h}(q,t) = \int_0^t e^{\nu q^2(\tau-t)}\hat{\eta}(q,\tau)d\tau. \tag{14}$$

The power spectrum is then $\langle \hat{h}(q,t)\hat{h}(-q,t)\rangle$, i.e.,

$$P(q) = 2F\frac{[1-\exp(-2\nu q^2 t)]}{\nu q^2}$$

for noncorrelated noise, and

$$P(q) = 2D_\rho q^{-2\rho}\frac{[1-\exp(-2\nu q^2 t)]}{\nu q^2},$$

for correlated noise. Using the expression of the power spectrum given by (12), We can calculate the surface width at each scale. We obtain for noncorrelated noise,

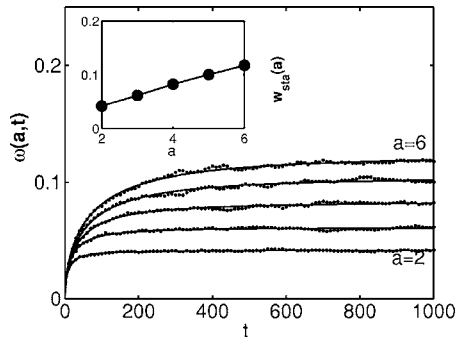

FIG. 3. The surface width as a function of time (dotted lines) for $a=2$, 3, 4, 5, and 6. The parameters used in this derivation are $\nu=0.1$ and $F=0.01$. Also shown, the fit to numerical data (continuous lines) using Eq. (17). The inset shows the linear dependence of the saturated width as a function of the scale as predicted by Eq. (17).

$$\omega_0(a,t)^2 = \int_0^{q_{\max}} \Gamma(a,q,t)dq = \frac{a^5 F\pi}{\nu}\int_0^{q_{\max}} (1-e^{-2\nu q^2 t})q^2 e^{-a^2q^2}dq \qquad (15)$$

and for correlated noise

$$\omega_\rho(a,t)^2 = \frac{2a^5 D_\rho \pi}{\nu}\int_0^{q_{\max}} q^{-2\rho+2}(1-e^{-2\nu q^2 t})e^{-a^2q^2}dq. \qquad (16)$$

The upper cutoff $q_{\max}$ is of the order of the inverse lattice constant; we assume that the correlation length is larger than $1/q_{\max}$ and we set $q_{\max}$ to infinity in (15) and (16), i.e.,

$$\omega_0(a,t)^2 = \frac{F\pi^{3/2}a^2}{\nu}\left[1-\left(1+\frac{2\nu t}{a^2}\right)^{-3/2}\right] \propto a^2 f_0\left(\frac{\nu t}{a^2}\right)^2 \qquad (17)$$

and

$$\omega_\rho(a,t)^2 = \frac{D_\rho \pi \Gamma\left(\frac{3}{2}-\rho\right)a^{2\rho+2}}{\nu}\left[1-\left(1+\frac{2\nu t}{a^2}\right)^{\rho-3/2}\right] \propto a^{2\rho+2} f_\rho\left(\frac{\nu t}{a^2}\right)^2, \qquad (18)$$

where $f_\rho(x)=\sqrt{[1-(1+2x)^{\rho-3/2}]}$. Thus, the dynamic exponent $z=2$ is independent of the nature of noise. On the other hand, the saturation value of the width depends on the nature of the noise and it scales as $\omega \propto a^\alpha$, with $\alpha=1$ for noncorrelated noise and $\omega \propto a^\alpha$ with $\alpha=\rho+1$ for spatially correlated noise. The result for white noise is obtained by setting $\rho=0$. The scaling function f_ρ has the asymptotic form $f_\rho(x) \propto x^{1/2}$ for $x \ll 1$ and $f_\rho(x) \to 1$ for $x \gg 1$.

IV. COMPARISON WITH NUMERICAL SIMULATION

A. Uncorrelated noise

We now consider the growth Eq. (2) with white noise source and solve it numerically. We compute the continuous wavelet transform of the obtained height profile using Eq. (10). The mother wavelet used is the Mexican hat wavelet $\psi(x)$. Then we compute the surface width of each decomposition directly using the formula

$$\omega(a,t)^2 = \frac{1}{L}\sum_{i=1}^{L}(WT_i(a,t)^2 - \overline{WT_i}(a,t)^2), \qquad (19)$$

where $\overline{WT_i}(a,t)$ is the average value at a given scale a. The index i refers to the position and L is the system size. We choose $L=10^6$. Figure 3 displays the evolution of the surface width for few decompositions, $a=2$, 3, 4, 5, and 6. The parameters used in this derivation are $\nu=0.1$ and $F=0.01$. The inset shows the linear dependence of the saturated width ($t \to \infty$), in agreement with Eq. (17). Note that in the early stages of growth, the surface width is independent of scale. To check the validity of the calculations derived in Sec. III, we fit the numerically determined surface width at a scale a with Eq. (17) for few different values of the scale a. The result is shown in Fig. 3. Clearly, the agreement between Eq. (17) and the numerical values of the surface width is very good. In Fig. 4 we plot $\omega(a,t)/a$ vs t/a^2 showing the data collapse, confirming the scaling relation (17).

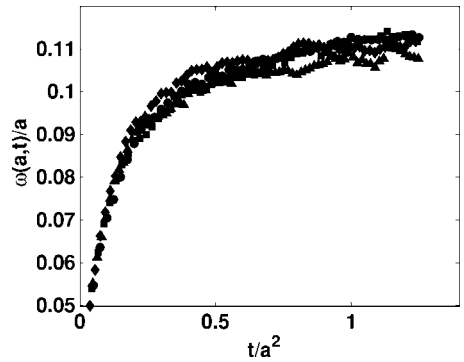

FIG. 4. Data collapse after rescaling, using $z=2$ and $\alpha=1$. Each symbol corresponds to a different scale, $a=2$ (●), $a=3$ (■), $a=4$ (▲), and $a=5$ (♦).

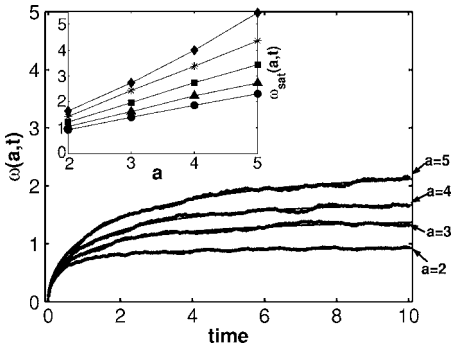

FIG. 5. The surface width as a function of time (dotted lines) for $a=2$, 3, 4, and 5. The parameters used in this derivation are $\nu=1$ and $F=0.01$. Also shown, the fit to numerical data (continuous lines) using Eq. (18). The inset shows the saturated width as a function of the scale as predicted by Eq. (18) for different values of $\rho=0.1$ (●), 0.2(▲), 0.3(■), 0.4(∗), and 0.48(♦).

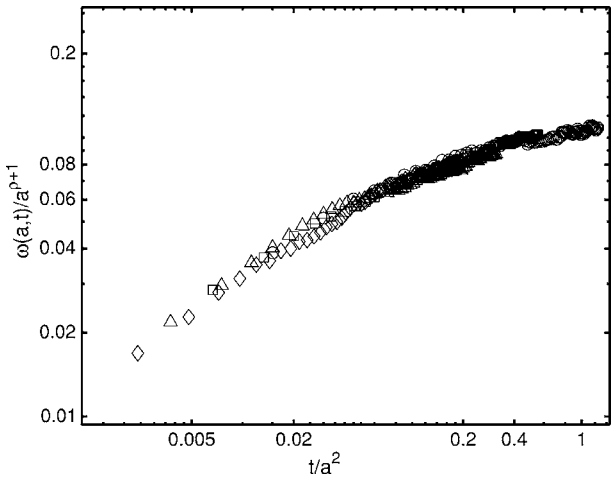

FIG. 6. Data collapse after rescaling data, in numerically solved EW equation with correlated noise using $z=2$ and $\rho=0.1$. Each symbol corresponds to a different scale: $a=2$ (◯), $a=3$ (△), $a=4$ (◇), and $a=5$ (□).

B. Correlated noise

We now numerically solve the EW equation but with correlated noise satisfying (4). To generate a correlated noise sequence, we use the same method used in Refs. [11,12] (note that other algorithms exist, see, for example, Ref. [13]), which is described as follows: we first generate an uncorrelated Gaussian noise $\eta(x,t)$, then we compute its Fourier transform $\hat{\eta}(q,t)$ and define

$$\hat{\eta}'(q,t) = q^{-\rho}\hat{\eta}(q,t). \tag{20}$$

Then we perform the inverse Fourier transform of $\hat{\eta}'(q,t)$ to obtain the correlated noise sequence $\eta'(x,t)$. Equation (2) is discretized using the standard backward forward difference numerical scheme. We choose the time step small enough to ensure convergence. The obtained surface profile is then wavelet transformed using $\psi(x)$ and the surface width is calculated for each scale using Eq. (19). Figure 5 displays the evolution of the surface width $\omega_\rho(a,t)$ for $\rho=0.1$. Also shown is the fit to Eq. (18) in which we set $\rho=0.1$. In the fit procedure, the parameters used in the numerical simulation (F and ν) are retrieved with an accuracy of about 10%. This discrepancy between the input values and the output ones is due to the discrete nature of the numerical procedure. The

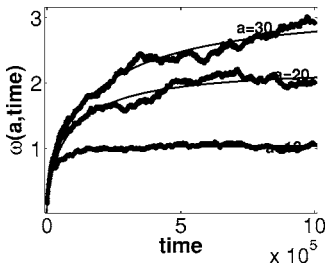

FIG. 7. Time evolution of the surface width (dotted lines) for three scales $a=10$, 20, and 30, for random deposition with relaxation. Also shown is the fit to Eq. (18) (continuous lines).

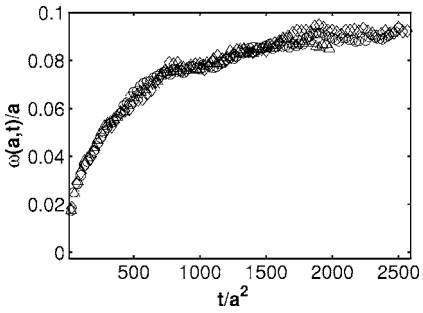

FIG. 8. Data collapse after rescaling in random deposition with relaxation, using $z=2$ and $\alpha=1$. Each symbol corresponds to a different scale, $a=10$ (◯), $a=20$ (△), and $a=30$ (◇).

inset of Fig. 5 shows the saturation value at each scale for different values of $\rho=0.2$, 0.3, 0.4, and 0.48. For small values of ρ, the distinction between different curves is hardly noticed since the exponents $\alpha=\rho+1$ are very close to each other. For $\rho=0.48$ the nonlinear relation (a power law relation) between ω_{sat} and the scale a becomes significant. Figure 6 shows the data collapse after plotting $w_p(a,t)/a^{\rho+1}$ vs t/a^2, confirming the scaling relation [Eq. (18)].

V. COMPARISON WITH A COMPUTER MODEL

In this section, we apply the results derived in Sec. III to a computer model which is believed to be described by the EW equation. This computer model was developed by Family and Viteck [14], to simulate random deposition, incorporating a surface relaxation mechanism. This model is described as follows: atoms are randomly falling on the surface where they are allowed to move (or diffuse) within a fixed length to positions where their height is at a minimum. Note that in our simulation, the computer-generated noise is uncorrelated, since each event is independent of the previous one. This is achieved by using a computer random numbers generator with uncorrelated sequence. Periodic boundary conditions are used in the present simulation. We set the system size to $L=10^8$ and the "diffusion length" to 5. The deposition is then carried out up to a time T. The wavelet transform of the height profile is then performed at different scales using the wavelet $\psi(x)$. Figure 7 shows the evolution of the surface width $\omega(a,t)$ for $a=10$, 20, and 30. Also shown, is the fit to Eq. (18). In this case, the agreement between analytical results and computer simulation is also very good. The scaling relation (18) is confirmed by the data collapsing procedure in which we plot $\omega(a,t)/a^{\rho+1}$ vs t/a^2. The result is shown in Fig. 8.

VI. CONCLUSION

In conclusion, we analyzed the dynamic scaling of EW growth model from the wavelets' perspective. EW equation is decomposed by applying a wavelet filter, discriminating the dynamics occurring at each scale. We investigated dynamic scaling in terms of scale but not the system size and derived the exact and simple expression for the scaling func-

tion. Two cases were considered, growth with correlated noise and growth with noncorrelated noise. We compared analytical solution for the surface width at each scale with numerical results and with computer simulation of deposition with relaxation. In both cases, there is a good agreement between theory, numerical, and computer simulations.

[1] *Dynamics of Fractal Surfaces*, edited by F. Family and T. Vicsek (World Scientific, Singapore, 1991).
[2] P. Meakin, *Fractals, Scaling and Growth far from Equilibrium* (Cambridge University Press, Cambridge, U.K., 1998).
[3] A. L. Barabasi and H. E. Stanley, *Fractal Concepts in Surface Growth* (Cambridge University Press, Cambridge, U.K., 1995).
[4] J. Krug and H. Spohn, *Solids far from Equilibrium: Growth Morphology and Defects* (Catena Verlag, Cremlingen-Destedt, 1987).
[5] S. F. Edwards and D. R. Wilkinson, Proc. R. Soc. London, Ser. A **381**, 17 (1982).
[6] T. Nattermann and L. H. Tang, Phys. Rev. A **45**, 7156 (1992).
[7] Y. K. Yu, N. N. Pang, and T. Halpin-Healy, Phys. Rev. E **50**, 5111 (1994).
[8] S. Majaniemi, T. Ala-Nissila, and J. Krug, Phys. Rev. B **53**, 8071 (1996).
[9] N. N. Pang, Phys. Rev. E **56**, 6676 (1997).
[10] T. Antal and Z. Rácz, Phys. Rev. E **54**, 2256 (1996).
[11] C. K. Peng, S. Havlin, M. Schwartz, and H. E. Stanley, Phys. Rev. A **44**, R2239 (1991).
[12] M. S. Li, Phys. Rev. E **55**, 1178 (1997).
[13] N. N. Pang, Y. K. Yu, and T. Halpin-Healy, Phys. Rev. E **52**, 3224 (1995).
[14] F. Family and L. T. Vicsek, J. Phys. A **18**, L75 (1985).